Shock formation in fluids having embedded regions of negative nonlinearity

M. S. Cramer and R. Sen

Citation: Physics of Fluids (1958-1988) **29**, 2181 (1986); doi: 10.1063/1.865555
View online: http://dx.doi.org/10.1063/1.865555
View Table of Contents: http://scitation.aip.org/content/aip/journal/pof1/29/7?ver=pdfcov
Published by the AIP Publishing

Shock formation in fluids having embedded regions of negative nonlinearity

M. S. Cramer and R. Sen
Engineering Science and Mechanics Department, Virginia Polytechnic Institute and State University, Blacksburg, Virginia 24061

(Received 3 January 1986; accepted 2 April 1986)

The steepening of one-dimensional finite-amplitude waves in inviscid Van der Waals gases is described. The undisturbed medium is taken to be unbounded, at rest and uniform. The specific heat is taken to be large enough to generate an embedded region of negative nonlinearity in the general neighborhood of the saturated vapor line and thermodynamic critical point. Under these conditions the shock formation process may differ significantly from that predicted by the perfect gas theory. The present study illustrates these differences for both isolated pulses and periodic wave trains. It is further shown that as many as three shocks, two compression and one expansion, may be formed in a single pulse or, in the case of wave trains, repeated element. It is also shown that the convected sound speed may become identical to the thermodynamic sound speed of the undisturbed medium at three distinct values of the density; the first of these corresponds to the density of the undisturbed medium while the other two are related to an integral of the fundamental derivative along an isentrope. The results obtained are expected to hold for any fluid which possesses such an embedded region of negative nonlinearity.

I. INTRODUCTION

The process of wave steepening and shock formation is of fundamental interest in nonlinear acoustic and gasdynamics. In single-phase Navier–Stokes fluids, the direction of steepening is determined by the thermodynamic parameter[1,3]

$$\Gamma = \Gamma(\rho,s) = \frac{1}{\rho}\frac{\partial(\rho a)}{\partial \rho}\bigg|_s, \tag{1}$$

where ρ is the fluid density, s is the entropy, and

$$a = a(\rho,s) = \left(\frac{\partial p}{\partial \rho}\bigg|_s\right)^{1/2} \tag{2}$$

is the sound speed; Eq. (1) is frequently referred to as the fundamental derivative of gasdynamics. When $\Gamma > 0$ everywhere in a wave train or pulse the wave steepens forward to form compression shocks, i.e., shocks in which the pressure of a fluid particle increases because of its encounter with the shock; when $\Gamma < 0$ the steepening is backward, which results in the formation of expansion shocks, i.e., shocks in which the pressure of a fluid particle decreases. The relation of (1) to the existence and permanence of compression and expansion shocks has been discussed by Bethe,[4] Zel'dovich,[5] Landau and Liftshitz,[6] Thompson,[2,3] and Thompson and Lambrakis,[7] among others. In accord with the results for shock formation, only compression shocks are possible in fluids having $\Gamma > 0$ and, when $\Gamma < 0$, expansion shocks are the only discontinuities satisfying the entropy inequality.

A second class of studies has attempted to determine the conditions under which $\Gamma < 0$. If the fluid is modeled as an ideal gas, it is well-known that the fundamental derivative is positive for all pressures and temperatures. However, this gas model is no longer valid as saturation conditions and, in particular, the thermodynamic critical point is approached, and a more accurate equation of state is needed. Bethe[4] and Zel'dovich[5] have shown that $\Gamma < 0$ for a range of pressures and temperatures in this region, provided the specific heats are sufficiently large. For purposes of illustration, the region of negative nonlinearity (i.e., where $\Gamma < 0$) has been computed for a Van der Waals gas and plotted in Fig. 1. Typical isentropes and the variation of the fundamental derivative along these isentropes are plotted in Figs. 2 and 3. As a continuation of this fundamental work, Thompson and Lambrakis[7] have employed more accurate equations of state to give examples of fluids that may exhibit negative nonlinearity. These were seen to include hydrocarbons and fluorocarbons of moderate complexity. The recent shock tube experiments of Borisov *et al.*[8] have provided direct evidence of expansion shocks in Freon-13, although this is likely to be related to the well-known anomalous behavior of the specific heats and sound speed in the vicinity of the critical point.

Negative nonlinearity is seen to occur in other areas of mechanics and physics. Thompson *et al.*[9] have observed expansion shocks in vapor–liquid mixtures, and Kynch[10] and Kluwick[11] describe negative nonlinearity in suspensions. It is well-known[12–15] that second sound waves in superfluid ^{4}He exhibit negative nonlinearity. In a related study, Garrett[16] has described positive and negative nonlinearity in ^{3}He-B. Evidences of negative nonlinearity in fused silica have been reported by Barker and Hollenbach[17] and Bains and Breazeale.[18] Lee-Bapty,[19] (see also the review by Crighton[20]) has shown that negative nonlinearity occurs in torsional waves in Kelvin–Voigt solids.

If Γ is negative everywhere in a given wave or wave train, it is expected that the wave evolution is essentially the same as that for $\Gamma > 0$; the main difference is that most of the standard gasdynamics inequalities need to be reversed. However, in many cases of interest, the local value of Γ may change sign within the same pulse or wave train. When this occurs, the phenomena observed may be qualitatively different than that seen when Γ does not change sign.[7,21,22] Analogous remarks hold in the areas of superfluid hydrodynamics[16,23–25] and wave propagation in suspensions[11] and viscoelastic materials.[19,20] Of direct interest to the present study are the shock formation computations of Cramer and Kluwick.[21] The medium was taken to be a single-phase Na-

 0031-9171/86/072181-11$01.90

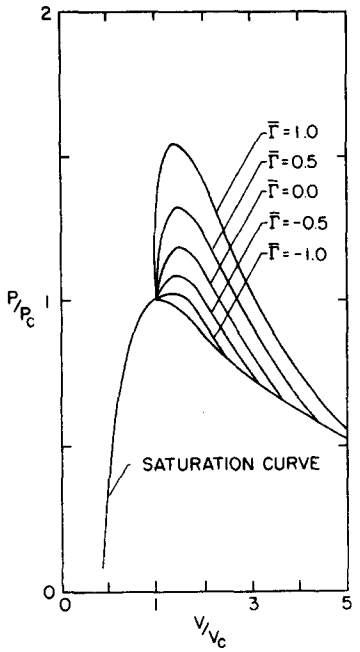

FIG. 1. Constant $\bar{\Gamma}$ contours for the Van der Waals gas with $\delta = 0.02$. Here V denotes the specific volume.

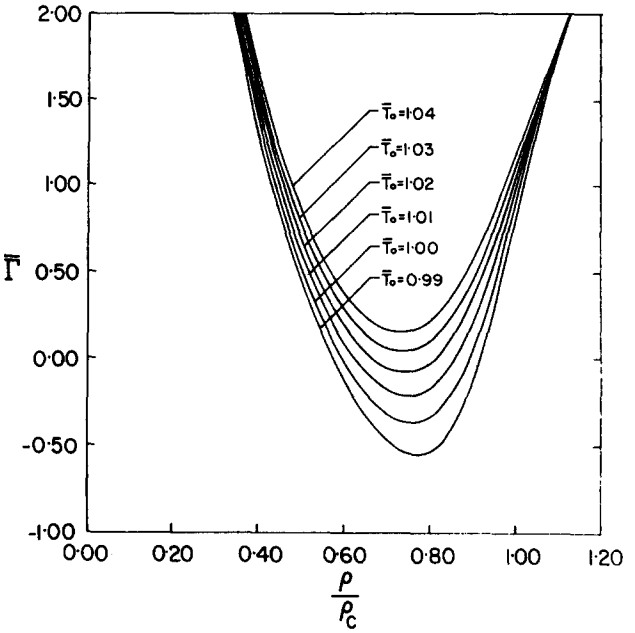

FIG. 3. Variation of $\bar{\Gamma}$ along isentropes of Fig. 2.

vier–Stokes fluid with undisturbed state in the vicinity of the $\Gamma = 0$ locus, see, e.g., Fig. 1 of the present study. Although the density perturbations were taken to be small compared to the density of the undisturbed medium, the amplitudes were large enough to result in part of the wave having $\Gamma > 0$ and the remainder having $\Gamma < 0$. Portions of the wave therefore steepen backward while other portions steepen forward. This results in a complicated evolution leading to the formation of compression and expansion shocks within the same pulse. Furthermore, it was shown that a maximum of two shocks can form in small-amplitude pulses.

The present study extends the work of Cramer and Kluwick[21] by describing the shock formation process in inviscid Van der Waals gases. The work of Bethe,[4] Zel'dovich,[5] and Thompson and Lambrakis[7] strongly suggests that the behavior of Γ predicted by this gas model gives a qualitatively correct picture for all fluids having regions of negative nonlinearity. Thus, we expect that our conclusions concerning the qualitative behavior will be applicable to most single-phase fluids that possess regions of negative nonlinearity.

In addition to the fundamental interest in this phenomenon, motivation for this study also comes from the role of wave steepening in the experimental determination of negative nonlinearity in various materials.[8,18] In single-phase fluids, wave steepening and the resultant harmonic generation would appear to be a relatively simple way to detect negative nonlinearity through use of either standing or progressive waves. Shock tube studies which attempt to detect negative nonlinearity may also involve wave distortion. In such studies it is possible and, in fact, likely that the shock waves, centered fans, or shock–fan combinations generated will take the flow from a region of positive to negative nonlinearity or vice versa. When this system reflects from an end wall and propagates into its former downstream state, it is clear that a complicated readjustment must occur. The present study is merely a first step toward understanding these phenomena.

The problem statement and exact equations governing the shock formation are given in the next section. This is followed by the specialization to the Van der Waals gas in Sec. III. The detailed description of the distortion of triangle pulses and sinusoidal wave trains is given in Secs. IV and V. There it is shown that as many as three shocks may form in a single wave. We expect that the formation of some shocks may be influenced and even prevented by the shocks formed at earlier times. The possible limitations resulting from these effects are discussed and estimated in Sec. VI.

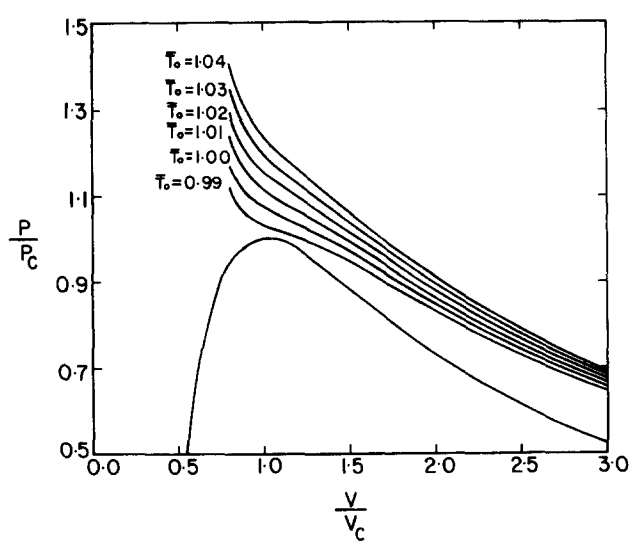

FIG. 2. Computed isentropes for the Van der Waals gas with $\delta = 0.02$. In this figure, $\bar{T}_*$ is simply a reference temperature which distinguishes one isentrope from another. The actual isentrope is computed from (21) and (25). The isentrope used for all examples corresponds to $\bar{T}_* = 1$.

II. PROBLEM STATEMENT AND GENERAL SOLUTION

We consider a single-phase Navier–Stokes fluid which, in the undisturbed state, is uniform and at rest; quantities evaluated at this undisturbed state are denoted by a subscript 0. The body force as well as any dissipative effects are ignored. At $t = 0$, a one-dimensional density distribution given by

$$\rho = \rho(x,0) = \rho_0[1 + AF(x/L)] \tag{3}$$

is assumed to exist in the fluid. All motions generated by this initial condition are also taken to be one-dimensional, i.e., the dependent variables reduce to position x and time t. Here A and L are measures of the amplitude and length of the disturbance and F is a sufficiently smooth nondimensional function of its argument. The disturbance is assumed to be isentropic, i.e., $s = s_0 = \text{const}$ and, to simplify the analysis, a right-moving simple wave. Thus, the corresponding velocity distribution is taken to be

$$v = v(x,0) = \int_{\rho_0}^{\rho(x,0)} \frac{a(r,s_0)}{r}\,dr, \tag{4}$$

where a is the sound speed given by (2). With these assumptions, the method of characteristics yields the exact parametric solution governing the evolution of the disturbance. If we define x_0 as the value of x at which each characteristic line intersects the $t = 0$ axis in the x-t plane, this exact solution requires

$$v(x,t) = v(x_0,0), \quad \rho(x,t) = \rho(x_0,0) \tag{5a}$$

on characteristic lines

$$x = x_0 + (a_0 + \sigma(\rho;\rho_0))t, \tag{5b}$$

where

$$\sigma(\rho;\rho_0) \equiv \int_{\rho_0}^{\rho} \Gamma(r,s_0)\,dr \tag{6}$$

is referred to as the convected sound speed and $a_0 \equiv a(\rho_0,s_0)$ and the functions $\rho(x_0,0)$, $v(x_0,0)$, and $\Gamma(\rho,s)$ are defined in (3), (4), and (1), respectively. Equation (5) states that the simple wave remains simple, and therefore v and ρ are constant on characteristic lines having constant slope equal to σ. The fact that (6) is in fact the convected speed is easily verified by integration by parts followed by use of the first equation of (5a) combined with (4).

Inspection of (6) verifies the expected result that $\sigma \to 0$ as $\rho \to \rho_0$, i.e., the speed of any disturbance approaches the sound speed of the undisturbed medium as $\rho \to \rho_0$. A more interesting observation is that σ may also become zero and change sign at two other values of ρ. Inspection of Fig. 3 reveals that this is caused by a balance of areas under the Γ-ρ curve. In all that follows we denote the zeroes of Γ by ρ_r and ρ_l such that

$$\begin{aligned} &\Gamma(\rho,s_0) \leqslant 0 \text{ for } \rho_l \leqslant \rho \leqslant \rho_r, \\ &\Gamma(\rho,s_0) > 0 \text{ otherwise.} \end{aligned} \tag{7}$$

If $\rho_l < \rho_0 < \rho_r$ the sound speed σ will always change sign if the disturbance is of sufficiently large amplitude. If $\rho_0 > \rho_r$ or $\rho_0 < \rho_l$, σ may or may not change sign depending on the total negative area available. For example, if $\rho_0 < \rho_l$, σ will change sign only if

$$\int_{\rho_0}^{\rho_l} \Gamma(r,s_0)\,dr < \left| \int_{\rho_l}^{\rho_r} \Gamma(r,s_0)\,dr \right|$$

is satisfied. This turns out to be the case when $\bar{T}_* = 0.99$ and 1.00 in Figs. 3 and 4. In the cases $\bar{T}_* = 1.01$ and 1.02, Γ changes sign but the area accumulated in integrating from ρ_0 to ρ_l is greater than the total amount of negative area between ρ_l and ρ_r. Had we chosen ρ_0 somewhat closer to ρ_l, these cases would also have resulted in a range where $\sigma < 0$. In the cases $\bar{T}_* = 1.03$ and 1.04, Γ remains positive and sign changes in σ are not even possible. It is also of interest to note that

$$\frac{d\sigma}{d\rho} = \Gamma(\rho,s_0),$$

thus, ρ_r and ρ_l will always correspond to either the maximum or minimum values of the convected sound speed σ. It should be noted that this nonmonotonic behavior of σ will always occur when Γ changes sign and is not dependent on the specific gas model. Maxima and minima in the characteristic slopes were seen to play a key role in the weak shock theory of Cramer and Kluwick[21] and Cramer, Kluwick, Watson, and Pelz.[22] Because of the small-amplitude approximation, the fundamental derivative changes sign only once and the resultant wave evolution is much simpler.

Once the specific heat, equation of state, and function F are specified, Eqs. (5) and (6) may be used to compute the wave evolution. It is well known that the straight characteristic lines [Eq. (5b)] intersect and cross each other, resulting in triple-valued solutions. Adjacent characteristics in the neighborhood of $x = x_0$, $t = 0$ intersect at time

$$t = [Q(x_0)]^{-1},$$

where

$$Q(x_0) \equiv -(A\rho_0/L)F'(x_0/L)\Gamma(\rho(x_0,0),s_0), \tag{8}$$

and $F'(\xi) \equiv dF(\xi)/d\xi$. The shock formation time is defined as the first time at which this occurs and therefore corre-

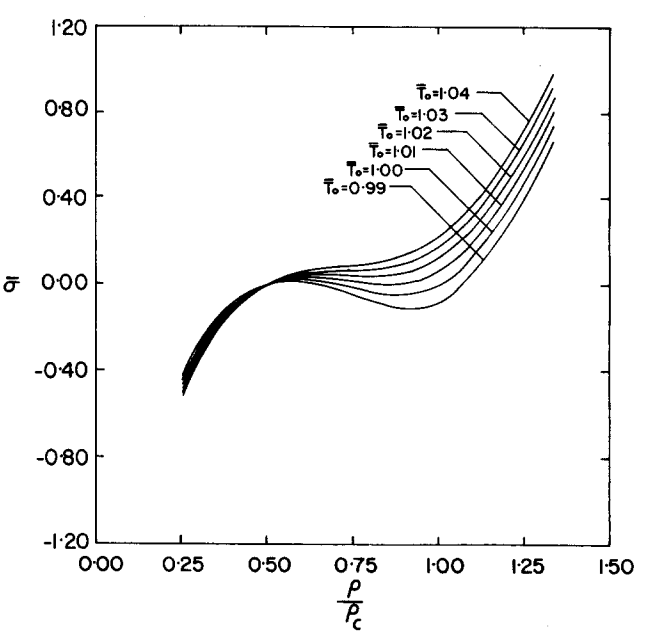

FIG. 4. Variation of $\bar{\sigma}$ along isentropes of Fig. 2 for $\bar{\rho}_0 = 0.5$. The $\bar{T}_* = 1$ curve exactly corresponds to the speed variation in Figs. 5–10.

sponds to the local maximum of Q with respect to x_0. If $\hat{x}_0$ is the value of x_0 at which Q has a positive maximum, the shock formation time is given by

$$\hat{t} = [Q(\hat{x}_0)]^{-1}. \tag{9}$$

It is useful to note that the value of $\hat{x}_0$ may be used to determine the characteristic at which the shock forms, i.e., the portion of the initial waveform which first steepens to form the shock.

The initial conditions are chosen to illustrate the evolution of isolated pulses and wave trains in as simple a manner as possible. To illustrate pulses, we employ the triangle wave defined by

$$F(\xi) \equiv \begin{cases} 2\xi + 1 & -\frac{1}{2} \leqslant \xi \leqslant 0, \\ -2\xi + 1 & 0 \leqslant \xi \leqslant \frac{1}{2}, \\ 0 & \text{otherwise}, \end{cases} \tag{10}$$

and, to illustrate wave trains, we employ the sine wave defined by

$$F(\xi) = \sin 2\pi\xi \tag{11}$$

for all ξ. The motivation for the choice of the latter has been discussed in the previous section. The motivation for (10) is that the effects of the variation of Γ and, in particular, the local minimum may be illustrated directly and clearly without having to allow for the effects of slope variations. A smooth profile, e.g., $F(\xi) = \operatorname{sech}^2 \xi$, will result in the same qualitative features although at the expense of some clarity of presentation.

III. VAN DER WAALS GASES

The equation of state[26] for a Van der Waals gas is

$$p = \rho RT/(1 - b\rho) - a\rho^2, \tag{12}$$

where T is the absolute temperature and a, b, R are positive constants related to the critical density ρ_c, pressure p_c, and temperature T_c by

$$\rho_c = \frac{1}{3b}, \quad p_c = \frac{a}{27b^2}, \quad RT_c = \frac{8a}{27b}. \tag{13}$$

The quantity R is the usual gas constant found in the theory of ideal gases and a and b account for the intermolecular forces and molecule size, respectively. In all that follows we apply (12) in the region outside of the mixed phase region under the saturation curve plotted in Figs. 1 and 2. As a result, the commonly assumed condition of mechanical stability[7,27]

$$\left.\frac{\partial p}{\partial \rho}\right|_T > 0$$

will always be satisfied.

The description of the fluid is complete once we specify the dependence of the specific heat at constant volume on the temperature. The density dependence is obtained through the well-known compatibility condition on the internal energy.[26] In the case of a Van der Waals gas, we find

$$C_v = C_v(T) \text{ only} > 0.$$

The latter inequality is the usual condition of thermal stability.[7,27] The precise dependence of C_v on temperature appears to have little influence on the wave evolution, at least in the present context. This is because of the fact that the gases which possess regions of negative nonlinearity typically have relatively large specific heats.[4,5,7] As a result, the temperature variation in an isentropic density variation is relatively small. Furthermore, in the case of Van der Waals gases, the specific heat nearly always appears as the ratio $R/C_v(T)$ [see, e.g., (15)–(17)] in the fundamental derivative and sound speed. Thus, the specific heat makes a relatively small contribution to the magnitude of Γ and a. The weak variations in C_v resulting from the temperature variations are therefore of even higher order. In the examples computed below, we therefore take

$$C_v = C_{v^*} = \text{const} \tag{14}$$

and large enough to result in the region of negative nonlinearity; see Thompson and Lambrakis[7] for a discussion of the estimates of the minimum values of C_v.

When we impose the condition (14), the sound speed (2) and fundamental derivative (1) of a Van der Waals gas are found to be

$$a^2 = \frac{RT(1+\delta)}{(1-b\rho)^2} - 2a\rho, \tag{15}$$

$$\Gamma = \frac{1}{2a\rho^2}\left(\frac{\rho RTZ}{(1-b\rho)^3} - 6a\rho^2\right), \tag{16}$$

where

$$Z = 2 + 3\delta + \delta^2 \tag{17}$$

and

$$\delta \equiv R/C_{v^*}. \tag{18}$$

The most convenient way to derive (15)–(17) is to first recast (1) and (2) in terms of density and temperature instead of density and entropy (see, e.g., Thompson and Lambrakis[7]). Differentiation of (12) and direct substitution then yields (15)–(17). By setting $a = b = 0$, it is easily verified that we recover the well-known results for perfect gases.

To determine the wave evolution, it will be necessary to evaluate (15)–(17) on an isentrope. The usual identities from thermodynamics[26] combined with (12) and (14) yield

$$s = s_* + C_{v^*} \ln\left(\frac{T}{T_*}\right) + R \ln\left(\frac{1-b\rho}{1-b\rho_*}\frac{\rho_*}{\rho}\right),$$

where the asterisk denotes quantities evaluated at an arbitrary reference state. Thus, along the isentrope given by $s = s_*$, the temperature is related to the density by

$$\frac{T}{T_*} = \left(\frac{1-b\rho_*}{1-b\rho}\frac{\rho}{\rho_*}\right)^{\delta}. \tag{19}$$

Thus, the variation of Γ along an isentrope may be obtained by substituting $T = T(\rho)$ from (19) into (15) and (16). This function of density may then be substituted in (9) and (5) to obtain the shock formation time and density distribution, respectively.

For purposes of presentation, it is convenient to recast our results in nondimensional terms. The thermodynamic variables of density, temperature, pressure, and entropy will be replaced by

$$\bar{\rho} \equiv \frac{\rho}{\rho_c}, \quad \bar{T} \equiv \frac{T}{T_c}, \quad \bar{p} \equiv \frac{p}{p_c}, \quad \bar{s} \equiv \frac{s - s_*}{C_{v^*}}, \tag{20}$$

respectively. As a result, the equation of state (12), sound speed (15), and fundamental derivative (16) and (17) of a Van der Waals gas may now be written

$$\bar{p} = 8\,\overline{\rho T}/(3-\bar{\rho}) - 3\bar{\rho}^2, \tag{21}$$

$$\bar{a}^2 = \frac{2}{3}\left(\frac{4\bar{T}(1+\delta)}{(3-\bar{\rho})^2} - \bar{\rho}\right), \tag{22}$$

$$\bar{\Gamma} = \frac{3}{\bar{a}}\left(\frac{4\bar{T}Z}{\bar{\rho}(3-\bar{\rho})^3} - 1\right), \tag{23}$$

where (13) has been used and

$$\bar{a} \equiv (b/\alpha)^{1/2} a, \quad \bar{\Gamma} \equiv (\alpha b)^{-1/2}\Gamma. \tag{24}$$

In all of the following we will regard $\bar{\Gamma} = \bar{\Gamma}(\bar{\rho},\bar{s})$: This is tantamount to regarding $\bar{T} = \bar{T}(\bar{\rho},\bar{s})$ in (22) and (23). The value of $\bar{\Gamma}$ on an isentrope $s = s_*$ will therefore be denoted by $\bar{\Gamma} = \bar{\Gamma}(\bar{\rho},0)$.

In terms of (20) the equation of the isentrope (19) reads

$$\frac{\bar{T}}{\bar{T}_*} = \left(\frac{3-\bar{\rho}_*}{2-\bar{\rho}}\,\frac{\bar{\rho}}{\bar{\rho}_*}\right)^{\delta}. \tag{25}$$

Equations (21) and (25) have been used to compute and plot the isentropes for $\delta = 0.02$, $\bar{\rho}_* = 0.5$, and various values of $\bar{T}_*$ in Fig. 2. Through use of (23) and (25) the variation in Γ along the same set of isentropes has been plotted in Fig. 3.

If we define nondimensional position and time by

$$\bar{X} \equiv \frac{x - a_0 t}{L}, \quad \bar{X}_0 = \frac{x_0}{L}, \quad \bar{t} \equiv \frac{a_0}{L}\,t, \tag{26}$$

we find that the parametric solution (5) may be rewritten as

$$\bar{\rho} = \bar{\rho}_0[1 + AF(\bar{X}_0)] \tag{27a}$$

on

$$\bar{X} = \bar{X}_0 + \bar{\sigma}(\bar{\rho};\bar{\rho}_0)\bar{t}, \tag{27b}$$

where

$$\bar{\sigma}(\bar{\rho};\bar{\rho}_0) = \frac{1}{3\bar{a}_0}\int_{\bar{\rho}_0}^{\bar{\rho}} \bar{\Gamma}(r,0)\,dr, \tag{28}$$

which is the nondimensional version of the convected sound speed. The integrand of (28) is obtained by combining (22) and (23) with the equation of the isentrope (25). Except in the ideal gas limit ($\bar{\rho}\to 0$), Eq. (28) must then be integrated numerically. This has been carried out for the set of isentropes plotted in Fig. 2 and the resulting variation of $\bar{\sigma}$ with $\bar{\rho}$ has been plotted in Fig. 4.

Finally, the nondimensional shock formation time is

$$\hat{\bar{t}} = [\bar{Q}(\hat{\bar{X}}_0)]^{-1}, \tag{29}$$

where $\hat{\bar{X}}_0$ are the values of $\bar{X}_0$ at which

$$\bar{Q}(\bar{X}_0) = (\bar{\rho}_0/3\bar{a}_0)\bar{\Gamma}(\bar{\rho}(\bar{X}_0,0),0)F'(\bar{X}_0) \tag{30}$$

has a positive local maximum. Typical functions $\bar{Q}$ have been computed and plotted in Fig. 5.

In each of the following specific examples, the entropy of the undisturbed state will be taken to be the same. That is, each undisturbed state will be taken to lie on the same isentrope. The isentrope chosen is that corresponding to $\bar{\rho}_* = 0.5$ and $\bar{T}_* = 1$ and is plotted in Fig. 2. To further simplify the comparisons we have scaled the nondimensional density distribution with its maximum value A. Thus, all plots will be of

$$u = (\bar{\rho} - \bar{\rho}_0)/\bar{\rho}_0 A \text{ vs } \bar{X},$$

which yields a maximum value of u equal to 1.

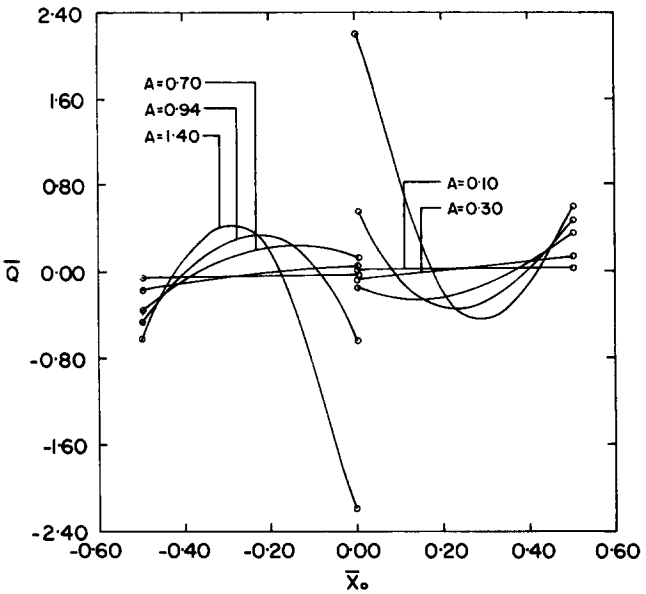

FIG. 5. Variation of $\bar{Q}$ with $\bar{X}_0$ for triangle wave. The undisturbed state is given by $\bar{\rho}_0 = 0.5$, $\bar{T}_0 = 1$, $\bar{p}_0 = 0.85$, $\bar{\Gamma} = 0.516$.

IV. TRIANGLE WAVES

The number of shock waves generated by the triangle wave [(3) and (10)] will depend on the state of the undisturbed fluid. Whenever the variation in Γ is similar to that of Fig. 3, the maximum number of shocks will be three when $\rho_0 < \rho_l$, two when $\rho_l < \rho_0 < \rho_r$, and one when $\rho_r < \rho_0$.

The first case is illustrated in Figs. 5–10 for the Van der Waals gas. The nondimensional density, temperature, pressure, and fundamental derivative of the undisturbed state are

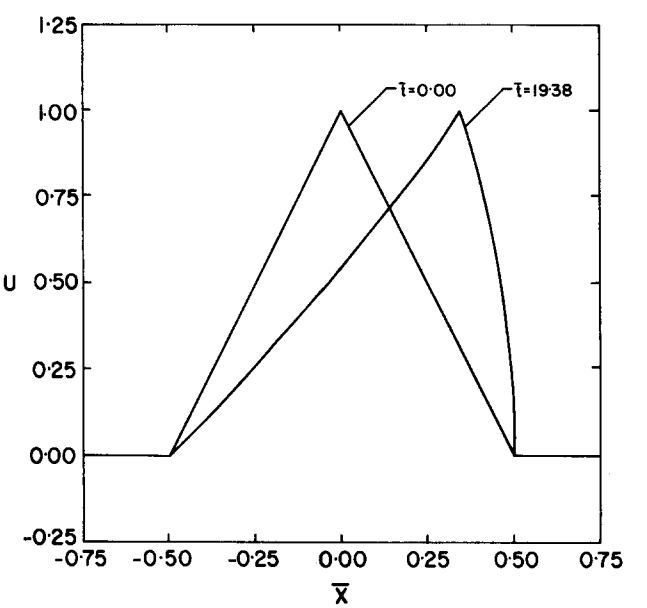

FIG. 6. Density distribution at formation time. Triangle wave, $A = 0.1$. Compression shock formed at $\bar{X}_0 = 0.5$.

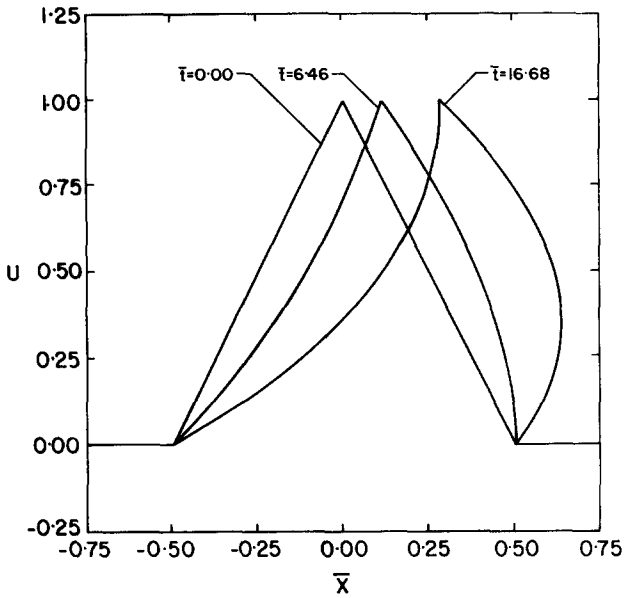

FIG. 7. Density distribution at formation times. Triangle wave, $A = 0.3$. Compression shock forms at $\bar{t} = 6.46$, $\bar{X}_0 = 0.5$, expansion shock at $\bar{t} = 16.68$, $\bar{X}_0 = 0$.

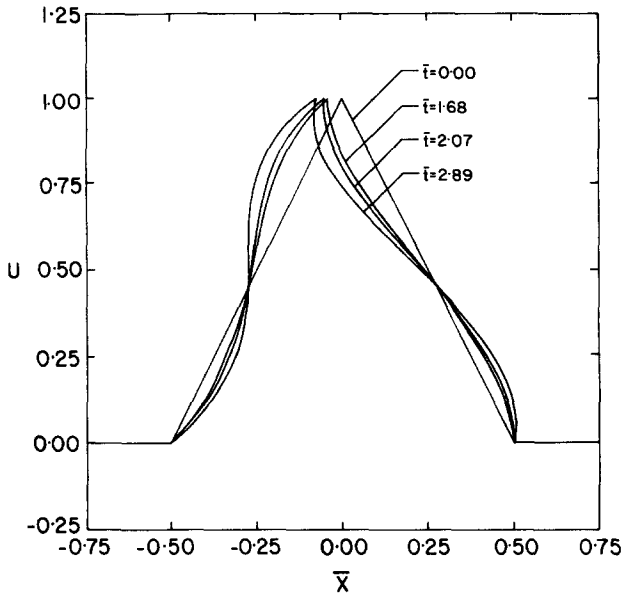

FIG. 9. Density distribution at formation times. Triangle wave, $A = 0.94$. Compression shocks form at $\bar{t} = 1.68$, $\bar{X}_0 = 0$ and $\bar{t} = 2.07$, $\bar{X}_0 = 0.5$, expansion shock at $\bar{t} = 2.89$, $\bar{X}_0 = -0.23$.

$$\bar{\rho}_0 = 0.5, \quad \bar{T}_0 = 1, \quad \bar{p}_0 = 0.85, \quad \bar{\Gamma}_0 = 0.516.$$

The peak amplitude A is varied from relatively small values to relatively large values. For each choice of A the function $\bar{Q}$ is plotted in Fig. 5.

In Fig. 6 we have plotted the density distribution at the shock formation time, $\bar{t} \approx 19.38$, for the case $A = 0.1$. Here Γ is positive at every point in the triangle wave, and the wave therefore steepens forward to form a single compression shock. As the wave amplitude is increased, the portion of the wave in the vicinity of the peak eventually enters the region of negative nonlinearity; for this particular case, this occurs when $A = 0.19$. This portion of the wave then steepens backward and an expansion shock forms near the peak. For the case $A = 0.3$, the density distributions at the shock formation times are plotted in Fig. 7. Although the compression shock at the front of the wave always forms at $\bar{X} = \bar{X}_0 = 0.5$, the expansion shock will form exactly at the peak only if

$$\left.\frac{\partial \Gamma}{\partial \rho}\right|_s < 0$$

at every point in the wave. When the wave amplitude is so large that Γ attains its minimum within the triangle wave, the expansion shock forms at a point corresponding to

$$-0.5 < \bar{X}_0 < 0.$$

In the present example, this occurs when $A > 0.50$, approximately. A further illustration of this point may be obtained

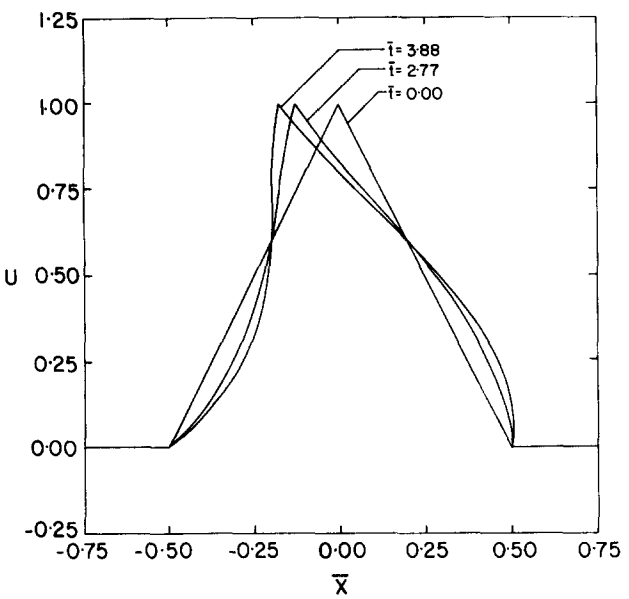

FIG. 8. Density distribution at formation times. Triangle wave, $A = 0.7$. Compression shock forms at $\bar{t} = 2.77$, $\bar{X}_0 = 0.5$, expansion shock at $\bar{t} = 3.88$, $\bar{X}_0 = -0.13$.

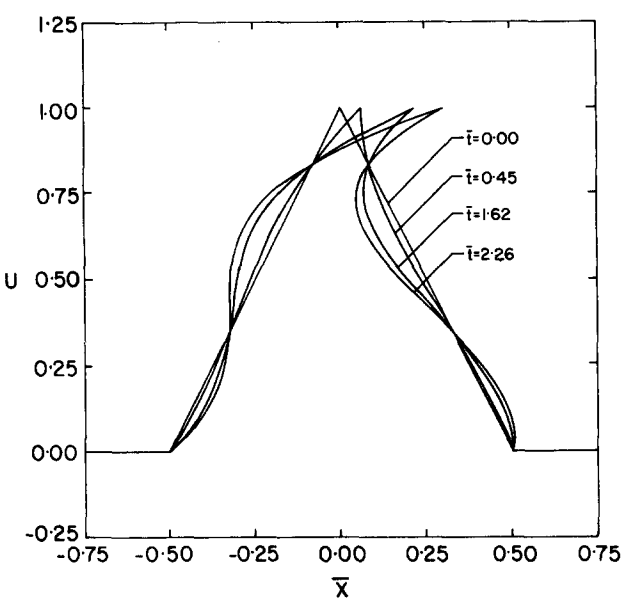

FIG. 10. Density distribution at formation times. Triangle wave, $A = 1.4$. Compression shocks form at $\bar{t} = 0.45$, $\bar{X}_0 = 0$ and $\bar{t} = 1.62$, $\bar{X}_0 = 0.5$, expansion shock at $\bar{t} = 2.26$, $\bar{X}_0 = -0.29$.

by comparing the variation of $\overline{Q}$ for the cases $A = 0.3$ and $A = 0.7$.

In Fig. 8 we have plotted the density distributions for the case $A = 0.7$. This differs from the previous case in that the convected sound speed (28) changes sign within the wave. This change in sign was discussed in Sec. II and is seen in Fig. 4.

In Figs. 9 and 10, the wave amplitude is so large that the peak of the wave extends into the region of positive nonlinearity $\rho > \rho_r$. In this particular case, the minimum value of A at which this occurs is approximately 0.89. Thus, a compression shock will now be formed at the peak resulting in a total of three shocks formed within the same wave. This last compression shock will always form at the peak, i.e., $\overline{X}_0 = 0$. In Fig. 10, the amplitude is so large that the convected wave speed $\bar{\sigma}$ changes sign again. At larger amplitudes, no qualitative changes are observed and the plots in Fig. 10 are typical of these larger amplitudes.

Comparison of Figs. 9 and 10 with the work of Cramer and Kluwick[21] reveals some of the limitations of the weak wave theory. Because the finite-amplitude wave is able to cross the $\Gamma = 0$ locus a second time, a third shock, not possible in the small-amplitude theory, is generated. The second change in sign in convected wave speed (28) is also not possible in Ref. 21.

Inspection of Figs. 8–10 suggests that the expansion shock consistently forms at the $\sigma = 0$ point. However, this is not the case and the fact that these points are close is merely coincidental. In these cases the expansion shock forms at the density corresponding to the minimum of Γ, i.e., where

$$\left.\frac{\partial \Gamma}{\partial \rho}\right|_s = 0,$$

see also Fig. 5. Inspection of (6) or (28) shows that this corresponds to the inflection point of the σ-ρ curve and will not, in general, be coincident with the $\sigma = 0$ point.

The second main case $\rho_l < \rho_0 \leqslant \rho_r$ is depicted in Figs. 11–13. The undisturbed state was taken to be on the isentrope of

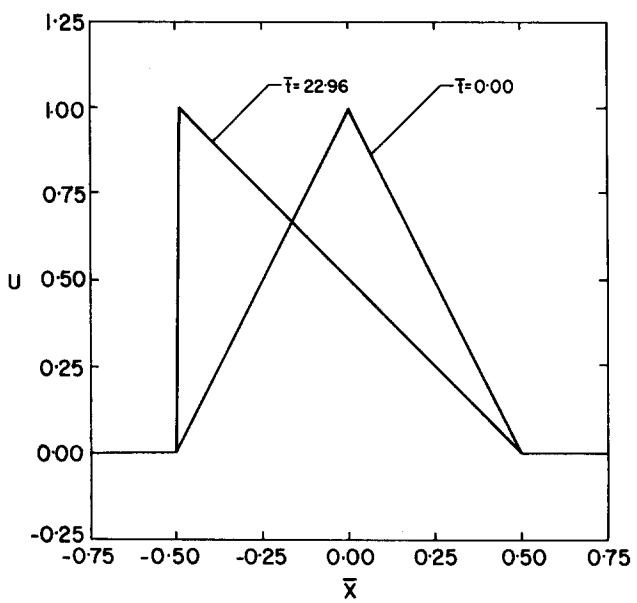

FIG. 11. Density distribution at formation time. Triangle wave, $A = 0.08$. Expansion shock forms at $\overline{X}_0 = -0.37$.

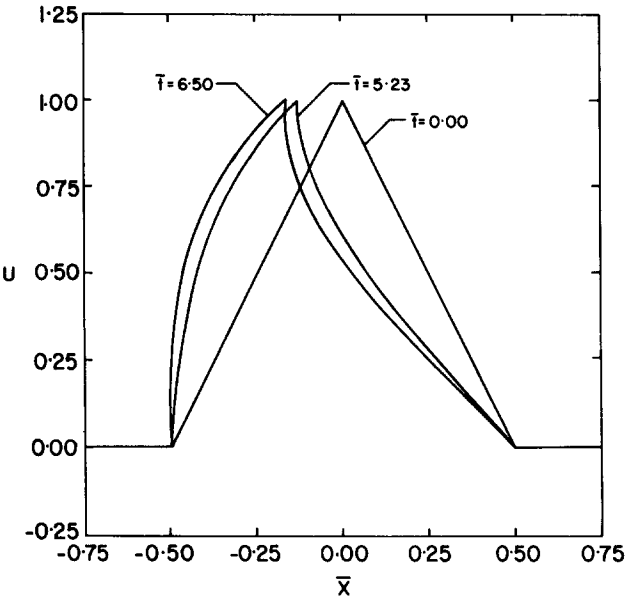

FIG. 12. Density distribution at formation times. Triangle wave, $A = 0.28$. Compression shock forms at $\bar{t} = 5.23$, $\overline{X}_0 = 0$, expansion shock at $\bar{t} = 6.50$, $\overline{X}_0 = -0.46$.

the previous case ($\bar{\rho}_* = 0.5$, $\overline{T}_* = 1$) with a nondimensional density equal to $\bar{\rho}_0 = 0.741$. The resultant nondimensional temperature, pressure, and fundamental derivative were found to be

$$\overline{T}_0 = 1.010, \quad \bar{p}_0 = 1.003, \quad \overline{\Gamma}_0 = -0.3635.$$

Figure 11 is typical of cases having relatively small amplitudes and therefore $\overline{\Gamma} < 0$ at every point in the wave. As expected, an expansion shock is formed along characteristics having $-0.5 < \overline{X}_0 < 0$. At larger amplitudes portions of the wave near the peak correspond to positive values of $\overline{\Gamma}$. Two typical cases are plotted in Figs. 12 and 13. In terms of time, the first shock formed is the compression shock at the peak

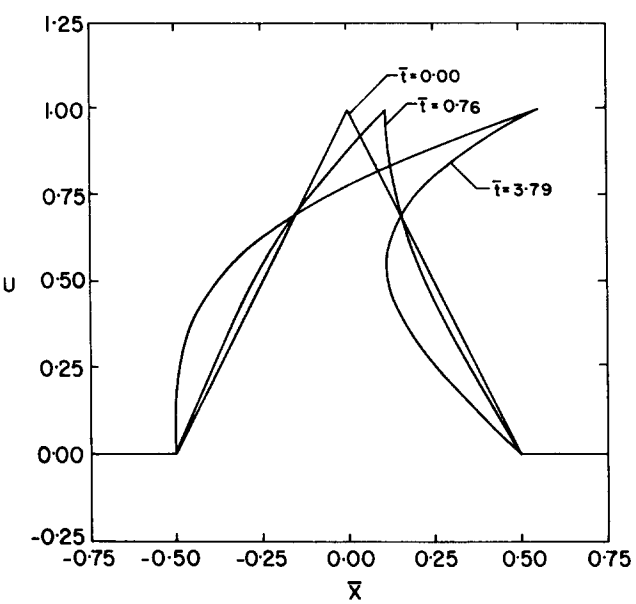

FIG. 13. Density distribution at formation times. Triangle wave, $A = 1.485$. Compression shock forms at $\bar{t} = 0.76$, $\overline{X}_0 = 0$, expansion shock at $\bar{t} = 3.79$, $\overline{X}_0 = -0.48$.

followed by the expansion shock at $-0.5<\bar{X}_0<0$. The last case is typical of the largest-amplitude cases and results in a change in sign in the convected sound speed $\bar{\sigma}$.

To complete our study of the triangle pulse we examine the last main case where $\rho_0>\rho_r$. Here $\bar{\rho}_0$ is taken to be 1.0. In order that the undisturbed state remains on the same isentrope as the previous cases, we must require that

$$\bar{T}_0=1.0185,\quad \bar{p}_0=1.074,\quad \bar{\Gamma}_0=0.918.$$

Because $\rho_0>\rho_r$, Γ will be positive for all positive values of A. A typical case has been plotted in Fig. 14.

In each of the main cases, the sequence described is typical of more general gases having embedded regions of negative nonlinearity. The only real difference occurs when the density of the undisturbed state is such that the area under the Γ-ρ curve cannot change sign, see, e.g., the discussion of Sec. II. In this case, the convected sound speed is always positive, although the number and type of shocks generated will remain the same.

V. PERIODIC WAVE TRAIN

When the initial condition is the sine wave defined in Sec. III, there are four main cases to be considered for arbitrary fluids having regions of negative nonlinearity. These correspond to density ranges

$$\begin{aligned}&\rho_0<\rho_l,\\&\rho_l<\rho_0<(\rho_r+\rho_l)/2,\\&(\rho_r+\rho_l)/2<\rho_0<\rho_r,\\&\rho_r<\rho_0.\end{aligned}\tag{31}$$

In each case a maximum of two compression shocks and one expansion shock may be formed.

In the first case, waves of relatively small amplitude have $\Gamma>0$ everywhere and a compression shock forms in the suction portion of the wave, i.e., portions having $\rho<\rho_0$. When the amplitude is large enough the compression portion of the wave, i.e., $\rho>\rho_0$, has $\Gamma<0$ and an expansion shock forms along characteristics having $0<x_0<L/4$. At even higher amplitudes a part of the compression phase extends into the region of positive nonlinearity $\rho>\rho_r$ and a second compression shock forms along characteristics in the range $L/4<x_0<L/2$.

The main difference between the last case listed ($\rho_0>\rho_r$) and the one just described is that it is in the suction phase (i.e., $\rho<\rho_0$ or $-L/2<x_0<-L/4$) rather than the compression phase, and that the value of Γ changes sign. Low-amplitude waves form a compression shock in the compression phase of the wave train. For larger-amplitude waves, the expansion shock is formed along characteristics corresponding to $-L/4<x_0<0$, and the second compression shock is formed in the suction phase.

In the second and third cases listed in (31), the undisturbed state is in the region of negative nonlinearity. The difference between these cases and the first and fourth cases is that both suction and compression phases will extend to regions of positive nonlinearity. The difference between the second and third cases is simply which portion of the wave leaves the region of negative nonlinearity first. We therefore will only give one specific example: This will correspond to the second case in (31). The undisturbed state is again taken to be on the same isentrope as in the previous section, i.e., $\bar{\rho}_*=0.5$ and $\bar{T}_*=1$, with $\bar{\rho}_0=0.690$. This requires that we take the nondimensional temperature, pressure, and fundamental derivative of the undisturbed state to be

$$\bar{T}_0=1.0089,\quad \bar{p}_0=0.9918,\quad \bar{\Gamma}_0=-0.3401.$$

For each value of the amplitude parameter A the variation in $\bar{Q}$ has been plotted in Fig. 15, and typical density distributions at the shock formation times have been plotted in Figs. 16–20.

The first plot (Fig. 16) is typical of relatively weak waves and results in the formation of a single expansion shock. As the wave amplitude is increased, the suction por-

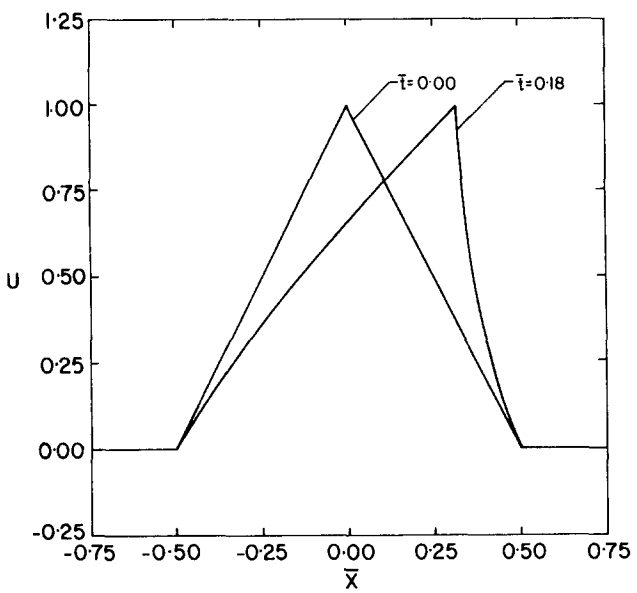

FIG. 14. Density distribution at formation times. Triangle wave, $A=0.6$. Compression shock forms at $\bar{X}_0=0$.

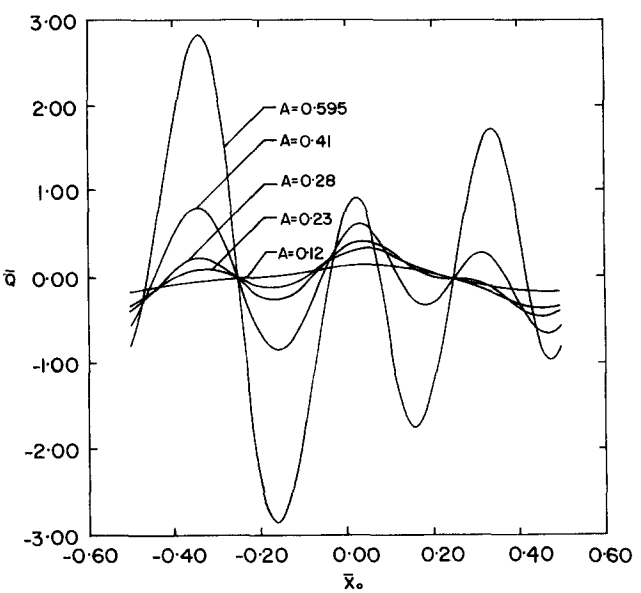

FIG. 15. Variation of $\bar{Q}$ with $\bar{X}_0$ for sinusoidal wave train. The undisturbed state is given by $\bar{\rho}_0=0.690$, $\bar{T}_0=1.0089$, $\bar{p}_0=0.9918$, and $\bar{\Gamma}_0=-0.3401$.

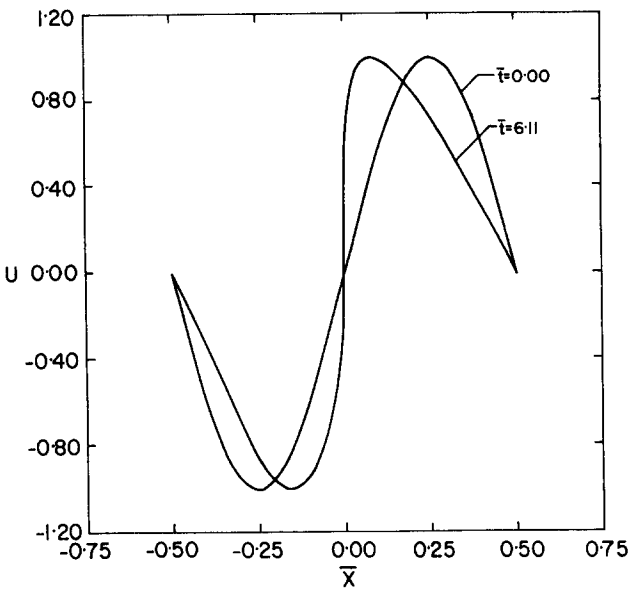

FIG. 16. Density distribution at formation time. Sinusoidal wave train, $A = 0.12$. Expansion shock forms at $\bar{X}_0 = 0.047$.

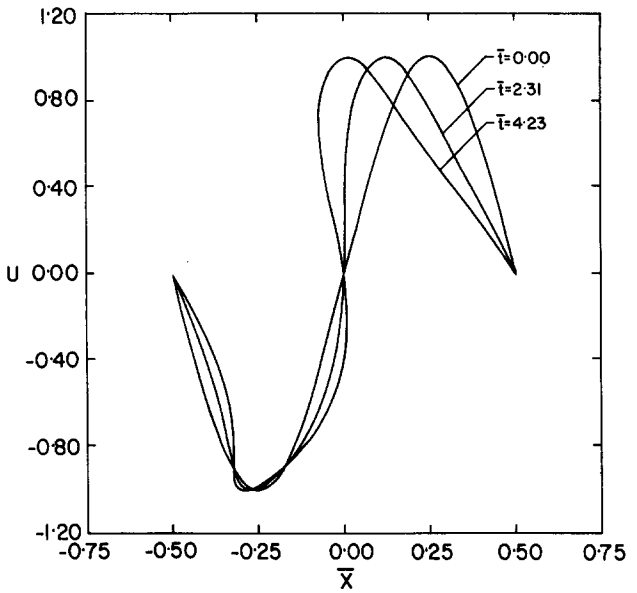

FIG. 18. Density distribution at formation times. Sinusoidal wave train, $A = 0.28$. Expansion shock forms at $\bar{t} = 2.31$, $\bar{X}_0 = 0.042$, compression shock at $\bar{t} = 4.23$, $\bar{X}_0 = -0.34$.

tion of the wave is the first to enter the region of positive nonlinearity. Thus, the compression shock is first formed in this portion of the wave as is indicated in Figs. 17 and 18. In Fig. 18, the wave amplitude has become large enough to result in a change in sign of the convected sound speed σ. At larger amplitudes the compression phase enters the region of positive nonlinearity corresponding to $\rho > \rho_r$ which results in the formation of a second compression shock in the compression portion of the wave. This brings the total number of shocks formed to three. These two large-amplitude cases are depicted in Figs. 19 and 20. The latter illustrates the expected change in sign in the convected sound speed. Also, compare the relative times of formation of the shocks in Figs. 18–20. At $A = 0.28$ (Fig. 18) the expansion shock forms first, whereas at $A = 0.41$ (Fig. 19) it forms second and finally third at $A = 0.595$ (Fig. 20). This progression is also seen in Fig. 15. There appears to be no simple criterion, such as that found in the weak shock theory,[21] for the relative formation times.

VI. LIMITATIONS CAUSED BY SHOCK DYNAMICS

Once a shock wave is formed, its motion and interaction with the remainder of the wave are a complicated nonlinear process. When the strength varies in time, entropy gradients and reflected waves are generated that lead to a violation of the simple wave assumption. However, it is well-known that these effects are negligible when the shock strength is small

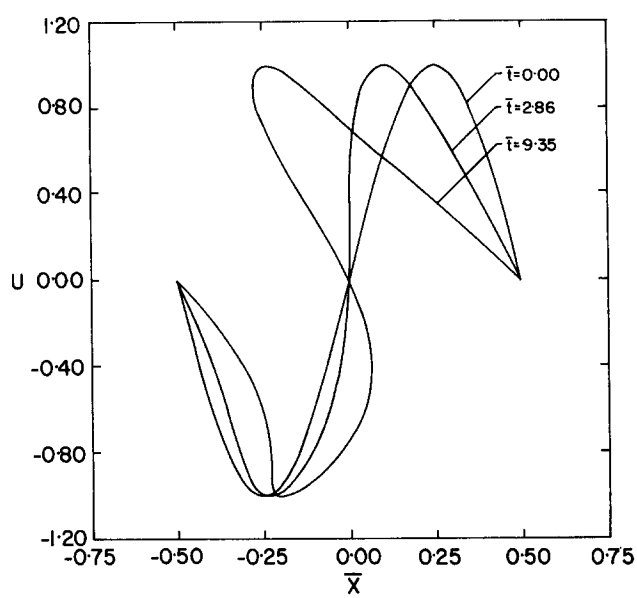

FIG. 17. Density distribution at formation times. Sinusoidal wave train, $A = 0.23$. Expansion shock forms at $\bar{t} = 2.86$, $\bar{X}_0 = 0.046$, compression shock at $\bar{t} = 9.35$, $\bar{X}_0 = -0.33$.

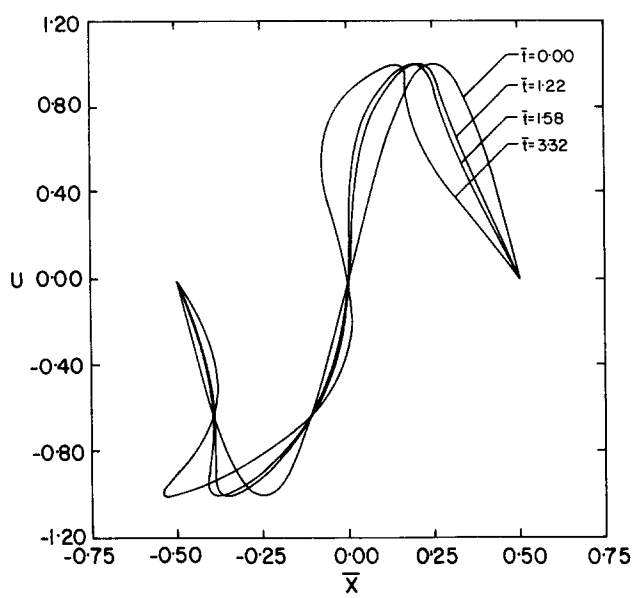

FIG. 19. Density distribution at formation times. Sinusoidal wave train, $A = 0.41$. Expansion shock forms at $\bar{t} = 1.58$, $X_0 = 0.033$. Compression shocks form at $\bar{t} = 1.22$, $\bar{X}_0 = -0.34$ at $\bar{t} = 3.32$, $\bar{X}_0 = 0.32$.

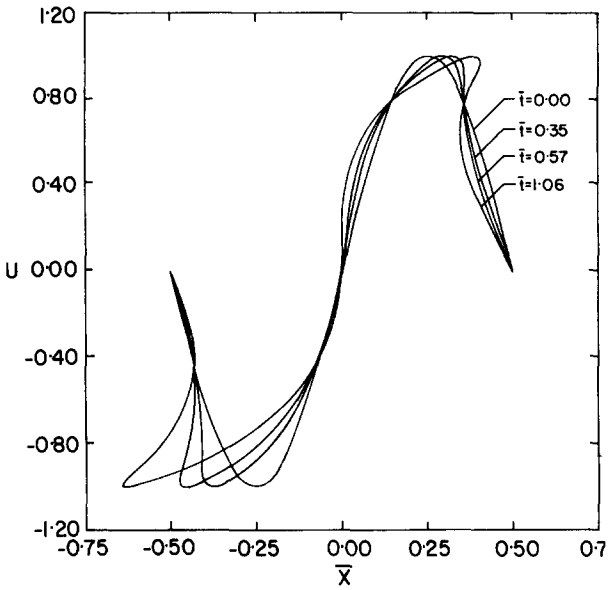

FIG. 20. Density distribution at formation times. Sinusoidal wave train, $A = 0.595$. Compression shocks form at $\bar{t} = 0.35$, $\bar{X}_0 = -0.34$ and $\bar{t} = 0.57$, $\bar{X}_0 = 0.34$. Expansion shock forms last at $\bar{t} = 1.06$, $\bar{X}_0 = 0.024$.

or even of moderate size. An excellent discussion of this point in the context of ideal gases is found in Chap. 6 of Whitham.[28] For a short period after the shock is formed, the strength is small and we therefore expect that these effects are negligible.

Thus, in general the formation of any particular shock will depend on the strength of any shock waves which have formed ahead of it. To estimate these effects for the cases presented here, we have computed the strength of the shock waves formed by an equal area rule. The entropy generated was then computed exactly. The equal area rule is only accurate when the shock is weak, i.e., the entropy jump is small. However, in all the cases examined, the latter was found to be the case and we conclude that our use of the area rule is at least self-consistent. More accurate computations based on the full method of characteristics will be presented in future studies. We have summarized the results for the sine wave initial conditions discussed in the last section in Table I. Here only the data for the strongest shocks in each figure are presented. The quantities $\bar{\rho}_1$, $\bar{\rho}_2$ are estimated from the equal area rule, and $\bar{p}_1$ and $\bar{\Gamma}_1$ are computed from (25) and (21)–(23). The downstream pressure may then be computed from the exact shock adiabat

$$\frac{[\bar{p}]}{\bar{p}_1} = (1-\zeta)\,\frac{1+\delta(3\bar{p}_1^2/\bar{p}_1\zeta)[\delta-1+(\bar{p}_1/3\zeta)(1+\zeta)]}{[(2+\delta)/2]\zeta-\bar{p}_1/3-\delta/2}$$

for Van der Waals gases. Here $\zeta \equiv \bar{\rho}_1/\bar{\rho}_2$ and brackets denote jumps in the indicated quantity. An equivalent formula has been given by Thompson and Lambrakis.[7] The downstream thermodynamic state $\bar{\rho}_2$, $\bar{p}_2$ is therefore known from which $\bar{T}_2$, $\bar{a}_2$, and $\bar{\Gamma}_2$ are computed from (21)–(23), respectively. From the exact expression for entropy used to derive (19), it can be shown that the nondimensional entropy jump across each shock is given by

$$\frac{[s]}{C_{v^*}} = \ln\left(\frac{\bar{T}_2}{\bar{T}_1}\right) + \delta \ln\left(\frac{3\zeta-\bar{\rho}_1}{3-\bar{\rho}_1}\right). \tag{32}$$

Inspection of these computed results shows that the entropy rise is very small in every case, and we conclude that these finite-amplitude effects will have little influence on the formation of shocks formed later in time. Similar conclusions were found for the triangle waves described in Sec. IV and have also been made by previous investigators.[7]

We have also displayed the upstream and downstream Mach numbers measured in a frame instantaneously moving with the shock. These were computed through use of mass conservation and the computed values of the sound speed (22). These show that the shock waves generated all satisfy the well-known speed ordering relation

$$M_1 > 1 > M_2$$

and that sonic shocks have not yet appeared.

Examination of the data for $\bar{\Gamma}$ in Table I shows that the expansion shock in Fig. 19 has $\bar{\Gamma} > 0$ at both the upstream and downstream states. The flow is shocked from the high-density, high-pressure region of positive nonlinearity across the $\bar{\Gamma} < 0$ region to the low-pressure region of positive nonlinearity. Such shocks are of a type similar to the double sonic shocks of Thompson and Lambrakis.[7] This suggests that a natural way to generate these double sonic shocks is through use of such periodic wave trains having an undisturbed state near the minimum value of $\bar{\Gamma}$.

A second consideration comes from the fact that the trajectory in the x-t plane of a generated shock crosses characteristic lines in its immediate neighborhood. Characteristic lines that converge may intersect the trajectory of a shock formed at an earlier time. Thus, the second shock will never form even though the characteristics cross. This may occur in the ideal gas theory although the initial conditions must be

TABLE I. Shock fitting data. The subscripts 1 and 2 denote conditions before and after the shock, respectively. The quantities $\bar{\rho}_1$ and $\bar{\rho}_2$ were obtained by application of an equal area rule to the indicated profile. In each case the profile used is that corresponding to the largest time. The compression shock used in the last example is that formed in the suction phase.

Shock	$\bar{\rho}_1$	$\bar{\rho}_2$	$(\bar{\rho}_2-\bar{\rho}_1)/\bar{\rho}_1$	$\bar{\Gamma}_1$	$\bar{\Gamma}_2$	$(s_2-s_1)/C_{v^*}$	M_1	M_2
Figure 17 Expansion shock	0.815	0.555	−0.129	−0.304	0.189	8×10^{-6}	1.071	0.981
Figure 18 Expansion shock	0.880	0.588	−0.120	−0.051	0.030	1×10^{-5}	1.079	0.961
Figure 19 Expansion shock	0.922	0.578	−0.135	0.232	0.078	2×10^{-5}	1.067	0.958
Figure 20 Compression shock	0.316	0.640	0.509	2.483	−0.169	2×10^{-4}	1.171	0.918

somewhat more complicated. The authors have also observed this phenomena using the weak shock theory of Cramer and Kluwick.[21] The formation and propagation of weak shocks in periodic triangle and sinusoidal wave trains were accurately computed, and it was found that the converging characteristics may or may not be overrun depending on the initial amplitude. A more complete analysis will be presented at a later date. On the basis of the equal area computations described above, we conclude that this has not occurred in any of the cases discussed here.

VII. CONCLUSIONS

The steepening and shock formation of finite-amplitude waves in Van der Waals gases have been examined. The specific heat was taken to be constant and large enough to result in a region of negative nonlinearity. Dissipative effects are ignored and the analysis is confined to the single-phase region indicated in Figs. 1 and 2. The results obtained are seen to be strikingly different from those obtained for ideal gases. In the latter case, the qualitative behavior is essentially the same for all amplitude ranges and states of the undisturbed fluid. The analysis and computations presented here show that Van der Waals gases exhibit a wide range of behavior which depend on the wave amplitude relative to the undisturbed state.

We have shown that as many as three shocks may be generated in triangle pulses and in periodic wave trains. A new shock is formed every time a portion of the wave crosses the $\Gamma = 0$ locus. Thus, if Γ changes sign once in a given waveform, we expect that two shocks, one compression and one expansion, will be formed; this is seen to be consistent with the weak shock theory.[21] Waves of larger amplitude may result in two sign changes in Γ and cannot be treated by the weak shock theory. When this is the case, we expect that the maximum of three shocks, two compression and one expansion, will be formed. We have also found that the convected sound speed σ may change sign twice, at most. This is seen to be caused by cancellations in the area under the Γ-ρ curve and is discussed in detail in Sec. II.

Studies by previous investigators[4,5,7] strongly suggest that results obtained for Van der Waals gases will be qualitatively correct for all fluids having a region of negative nonlinearity. The first author of the present study has carried out a complete analysis of the shock formation for fairly general equations of state. The only assumption on the form of the equation of state was that the region of negative nonlinearity be similar to that depicted in Figs. 1–3. That is, it is a tongue-shaped region in the pressure-specific volume plane with a variation of Γ along an isentrope qualitatively resembling that of Fig. 3. The conclusion obtained is that the general predictions discussed here do not depend on the specific equation of state but are expected to hold for any fluid exhibiting a region of negative nonlinearity of the type predicted by Bethe,[4] Zel'dovich,[5] and Thompson and Lambrakis.[7]

Although our goal is not to describe the shock evolution after formation, Sec. VI does provide a discussion of the influence of shocks already generated on the formation of other shocks at later times. On the basis of the equal area rule discussed in Sec. VI, we conclude that the examples presented in Secs. IV and V are accurate representations of the wave evolution. However, in general, one must always check for these effects when the overall wave amplitudes are finite.

[1] A. H. Shapiro, *The Dynamics and Thermodynamics of Compressible Fluid Flow* (Wiley, New York, 1953).
[2] P. A. Thompson, Phys. Fluids **14**, 1843 (1971).
[3] P. A. Thompson, *Compressible-Fluid Dynamics* (McGraw-Hill, New York, 1972).
[4] See National Technical Information Service Document No. PB 032189 (Office of Scientific Research and Development Rep. No. 545). Copies are available at the U.S. Library of Congress under the NTIS number.
[5] Ya. B. Zel'dovich, Zh. Eksp. Teor. Fiz. **4**, 363 (1946).
[6] L. D. Landau and E. M. Lifshitz, *Fluid Mechanics* (Addison-Wesley, Reading, MA, 1959).
[7] P. A. Thompson and K. C. Lambrakis, J. Fluid Mech. **60**, 187 (1973).
[8] A. A. Borisov, Al. A. Borisov, S. S. Kutateladze, and V. E. Nakoryakov, J. Fluid Mech. **126**, 59 (1983).
[9] P. A. Thompson, G. C. Carofano, and Y-G. Kim, J. Fluid Mech. **166**, 57 (1986).
[10] G. J. Kynch, Trans. Faraday Soc. **48**, 116 (1952).
[11] A. Kluwick (private communication).
[12] H. N. V. Temperley, Proc. Phys. Soc. London Sect. A **64**, 105 (1951).
[13] D. V. Osborne, Proc. Phys. Soc. London Sect. A **64**, 114 (1951).
[14] I. M. Khalatnikov, Zh. Eksp. Teor. Fiz. **23**, 253 (1952).
[15] A. J. Dessler and W. M. Fairbank, Phys. Rev. **104**, 6 (1956).
[16] S. Garrett, J. Acoust. Soc. Am. **60**, 139 (1981).
[17] L. M. Barker and R. E. Hollenbach, J. Appl. Phys. **41**, 4208 (1970).
[18] J. A. Bains and M. A. Breazeale, J. Acoust. Soc. Am. **57**, 745 (1975).
[19] I. P. Lee-Bapty, Ph. D. dissertation, Leeds University, 1981.
[20] D. G. Crighton, *Proceedings of the IUTAM Symposium on Nonlinear Deformation Waves* (Springer, Berlin, 1982), p. 115.
[21] M. S. Cramer and A. Kluwick, J. Fluid Mech. **142**, 9 (1984).
[22] M. S. Cramer, A. Kluwick, L. T. Watson, and W. Pelz, submitted to J. Fluid Mech.
[23] T. N. Turner, Ph. D. dissertation, California Institute of Technology, 1979.
[24] T. N. Turner, Physica **107B**, 701 (1981).
[25] T. N. Turner, Phys. Fluids **26**, 3227 (1983).
[26] C. J. Adkins, *Equilibrium Thermodynamics* (Cambridge U. P., Cambridge, MA, 1983).
[27] W. D. Hayes, Gasdynamic Discontinuities, *Princeton Series on High Speed Aerodynamics and Jet Propulsion* (Princeton U. P., Princeton, NJ, 1960).
[28] G. B. Whitham, *Linear and Nonlinear Waves* (Interscience, New York, 1974).